Prophages regulate *Shewanella fidelis* 3313 motility and biofilm formation: implications for gut colonization dynamics in *Ciona robusta*

Ojas Natarajan[1], Susanne L. Gibboney[1], Morgan N. Young[1], Shen Jean Lim[4], Natalia Pluta[2***], Celine G.F. Atkinson[3], Brittany A. Leigh[1,4*], Assunta Liberti[1,5], Eric D. Kees[7**], Mya Breitbart[4], Jeffrey A. Gralnick[6,7], and Larry J. Dishaw[1,3,4‡]

[1.] Morsani College of Medicine, Pediatrics, [2]Biomedical Sciences Program, [3]Department of Cell Biology, Microbiology, and Molecular Biology, [4]College of Marine Science, University of South Florida, Tampa, Fl USA, [5]Stazione Zoologica Anton Dohrn, Naples, Italy, [6]Plant and Microbial Biology, University of Minnesota, St. Paul, MN USA, [7]BioTechnology Institute, University of Minnesota, St. Paul, MN USA.
* Current address: LifeSci Communications, New York and Boston, USA.
** Current address: Cargill Corporation, Wayzata, MN, USA.
*** Current address: Uniformed Services University of Health Sciences, Bethesda, MD, USA
[‡] Corresponding author: ldishaw@usf.edu

Abstract

Lysogens are bacteria that contain viruses (prophages) integrated into their genomes, and these prophages often affect metabolic pathways and other traits of their bacterial hosts. Lysogens are abundant in the gut of animals. However, the potential influence of prophages on the gut microbiota-host immune axis in animals remains poorly understood. Here, we investigated the role of prophages in a marine lysogen, *Shewanella fidelis* 3313, a persistent member of the gut microbiome of the model tunicate, *Ciona robusta*. Deletion mutants were established for two prophages (SfMu1 and SfPat) to determine their impact on bacterial physiology *in vitro* and in the context of colonizing the *Ciona* gut. This study reveals the influence of prophages on bacterial traits that shape colonization dynamics. *In vitro*, these two prophages enhance *S. fidelis* 3313 motility and swarming while reducing biofilm formation. To understand the *in vivo* impact of these prophage-induced changes on bacterial traits, we exposed metamorphic stage 4 *Ciona* juveniles (the stage that correlates to first feeding and

subsequent gut colonization) to both wildtype (WT) and modified strains of *S. fidelis* 3313. During gut colonization, expression of the *pdeB* gene is upregulated in the WT strain but not the deletion mutants. PdeB is a phosphodiesterase that degrades cyclic-di-GMP, a dinucleotide messenger, which influences biofilm formation and motility. Colonization by the WT strain and increased expression of *pdeB* also correlate to the reduced expression of the *Ciona* gut immune effector, VCBP-C. Differential localization of the prophage deletion mutant strain to the stomach epithelium and the WT to the esophagus was observed upon colonization of the juveniles. Our findings highlight the importance of investigating inter-kingdom interactions between prophages, bacteria, and their animal hosts in regulating the gut microbiota-host immune axis.

Importance

The gut microbiome is now recognized to have important influences on host physiology. These host-associated microbial communities are often predominated by bacteria that carry prophages, which are bacteriophages (or phages) that stably integrate into bacterial genomes. While it is recognized that prophages can influence bacterial physiology, their impact on inter-kingdom dynamics in the gut of animals remains poorly understood. Here, we show that prophages contribute to increased motility and reduced biofilm formation in *Shewanella fidelis* 3313, a marine bacterium that colonizes the *Ciona robusta* gut. Prophages were also found to be associated with changes in the regulation of a bacterial secondary signaling molecule, cyclic di-GMP, and corresponded with variations in *Ciona* innate immune responses. Our work

highlights potential tripartite links between prophages, their bacterial hosts, and animal immune functions.

Introduction

The gastrointestinal tract (or gut) of animals is lined by an epithelial layer with a mucus-rich surface. This dynamic environment is a primary interface between host immunity, symbiotic microbes, and dietary antigens [1, 2]. In the process of colonizing the gut, bacteria encounter physical, chemical, and biological forces. They must compete for nutrients and niche space while managing the stress of digestive enzymes and host immune factors [3-6]. Gut-colonizing bacteria also encounter bacteriophages (phages), or viruses that infect bacteria [7]; e.g., over 10^{12} viruses have been estimated in the human gut [8].

Phages exhibit both lytic and temperate lifestyles. While the former is known to impact bacterial community dynamics through lysis, the impact of temperate phages on bacterial communities, particularly those that associate with animals, remains poorly understood. Conventionally, temperate phages integrate into bacterial genomes as prophages and remain ‘dormant’ until an external trigger activates them to enter the lytic cycle [9-11]; these bacteria are considered ‘lysogenized’ and referred to as lysogens [9, 10]. Prophages often encode accessory genes that can influence bacterial traits and behaviors [12]. These genes can encode virulence factors, antibiotic resistance genes, and those that provide superinfection exclusion, thereby protecting their bacterial hosts from infections by related phages [13]. Based on the site of integration, prophages can also impact the expression of bacterial genes [14]. Bacterial lysogens exist in every

environment [15-17] and are particularly prevalent in the microbiomes of diverse animals [8, 18].

Prophage induction results in bacterial lysis and can be mediated by various stressors, including antibiotics and inflammatory processes [19-27]. Because prophages can influence phenotypes, such as biofilm formation of their bacterial hosts [25], understanding the impact of lysogens in animal microbiomes is becoming a research priority [28-30]. In the gut, biofilms associated with host mucus may benefit the host by enhancing epithelial barriers against pathogenic invasion [31]. Integration of prophages into bacterial genomes may impart functional changes that could be important in surface colonization. For example, in *E. coli* K-12, integrating the Rac prophage into a tRNA thioltransferase region disrupts biofilm functions [32]; deleting this prophage decreases resistance to antibiotics, acids, and oxidative stress. Some of these traits may be regulated by prophage-specific genes [26]. Prophages have also been shown to influence biofilm lifecycles in *Pseudomonas aeruginosa* [33, 34].

Lysogenized *Shewanella* species colonize the gut of *Ciona robusta*, an ascidian collected in Southern California waters [35, 36] and from here on referred to as *Ciona*. Tunicates like *Ciona* are a subphylum (Tunicata) of Chordates that are well-established model systems for studies of animal development [37-39] and are now increasingly leveraged for gut immune and microbiome studies [40]. *Ciona* maintains stable gut bacterial and viral communities [17, 35] despite continuously filtering microbe-rich seawater and only possessing innate immunity. Previous efforts to define gut immunity in *Ciona* revealed the presence of a secreted immune effector, the variable immunoglobulin (V-Ig) domain-containing chitin-binding protein, or VCBP, that serves

important roles in shaping the ecology of the gut microbiome by binding bacteria and fungi (as well as chitin-rich mucus) on opposing functional domains [41, 42]. *Ciona* VCBP-C is one of the best-studied VCBPs, expressed in the stomach and the intestine and shown to bind bacteria *in vitro* and the gut lumen [42]. Based on various *in vitro* and *in vivo* observations, it was proposed that VCBPs likely modulate bacterial settlement and/or biofilm formation [40, 41, 43]. The potential influence of soluble immune effectors on host-bacterial-viral interactions is of considerable interest. However, the possibility that prophages may influence the interactions between bacteria and VCBPs remains to be explored. *Shewanella fidelis* strain 3313 was isolated previously from the gut of *Ciona*. It was shown to possess two inducible prophages, SfPat and SfMu [36], the latter of which is referred to as SfMu1 in the current manuscript. Furthermore, *in vitro* experiments demonstrated enhanced biofilm formation in *S. fidelis* 3313 in the presence of extracellular DNA (eDNA) that may originate from phage activity [36]. A link between phage-mediated lysis and biofilm formation has been demonstrated previously in other *Shewanella* species [34]. For example, in *S. oneidensis* strain MR-1, Mu and Lambda prophages enhance biofilm formation via eDNA released during prophage-induced lysis, with genomic DNA likely serving as a scaffold for biofilms [34]. Similarly, the P2 prophage of *S. putrefaciens* strain W3-18-1 influences biofilm formation via spontaneous induction at low frequencies, resulting in cell lysis and contributing eDNA that can mediate biofilm formation [44].

Here, we set out to characterize the influence of prophages, SfPat and SfMu1, on their host, *S. fidelis* 3313. The genome assembly for *S. fidelis* 3313 was further refined by combining both long-read and short-read sequencing, resulting in improved

resolution of the genomic landscape of the prophages and associated regions. We then designed a homologous recombination-based deletion strategy to generate mutants with one or both prophages deleted, i.e., knocked-out. We report that prophage deletion results in reduced bacterial motility and increased biofilm formation *in vitro*. During gut colonization *in vivo*, these behavioral changes may affect expression of bacterial genes encoding signaling molecules as well as important host innate immune genes. Colonization of the gut in laboratory-reared *Ciona* juveniles using wild-type (WT) and prophage knockout (KO) mutant strains suggested that the influence of prophages on the outcome of bacterial colonization of the gut is also impacted by host genetics. The results reported herein reflect complex inter-kingdom interactions among prophages, bacterial hosts, and animal immune systems.

Methods

Culture and growth conditions

S. fidelis 3313 used in this study was originally isolated from the gut of *Ciona robusta* obtained from Mission Bay, CA, USA, as previously described [36]. The bacterium was cultured using Difco marine agar 2216 (MA) (Fisher Scientific, Hampton, NH) and marine broth (MB) at room temperature. Subsequent genetic manipulations were performed on strains grown in LB/MB, which consists of a mixture of 75% LB (Lysogeny Broth, Fisher Scientific, Hampton, NH) and 25% MB. Strains are listed in Table 1.

Genome Assembly

Genomic libraries were prepared from isolated colonies on MA and grown in MB using NuGen Ovation Ultralow DNA kit (Eurofins, Louisville KY) for Illumina sequencing and SMRTbell II for PacBio sequencing. Samples were sequenced on the Illumina MiSeq 2x250 bp platform (San Diego, CA, USA) and PacBio SMRT Cell (Pacific Biosciences, Menlo Park, CA, USA). Illumina-sequenced reads were quality-trimmed at Q=30 with Trimmomatic v0.36 [45] and co-assembled with PacBio-sequenced reads using Unicycler v0.4.8 [46]. Genome completion, strain heterogeneity, and contamination were assessed using checkM v1.0.9 [47]. Whole genome amino acid identity (AAI) was used to identify or verify taxonomy using compareM v0.0.2.3 [48]. The assembled genome was annotated by the Rapid Annotation using the Subsystem Technology (RAST) server [49]. Identification and annotation of prophage-encoding genome regions was performed with a software pipeline that included PhiSpy, VirSorter, PHASTER and VIBRANT [50-53].

Prophage deletion

Two prophages, SfPat and SfMu1, were targeted for deletion from *S. fidelis* 3313 using homologous recombination methods adapted from Saltikov and Neuman [54] to produce single and double-knockout mutant strains. First, a pSMV3 suicide vector [54] was designed with ~700 bp regions corresponding to the upstream and downstream sequence of the prophages (Table 2). These flanking regions were amplified and ligated using overlap extension PCR, then directionally inserted into the vector with the restriction enzymes BamHI and SacI (Table 3) [55]. Plasmid conjugation was then

performed by inoculating a colony of *S. fidelis* 3313 into a culture of *E. coli* containing the desired suicide vector on an LB/MB agar plate for two hours.

To study the influence of prophages on *S. fidelis* 3313, two of the three prophages, SfPat and SfMu1, were targeted for deletion using homologous recombination. The third prophage, SfMu2, is larger (over 65 kb) and is being targeted as part of future efforts. To target SfMu1, primers EDK73/74 and EDK75/76 were designed to amplify 667 bp upstream and 752 bp downstream of the prophage (**Figure 1a**). Flanking primers EDK83/84 were used for PCR screening of candidate deletion clones, amplifying 1607 bp in the event of a successful deletion and yielding no product in case of an unsuccessful deletion as the product is too large to amplify. To target SfPat, primers EDK77/78 and EDK79/80 were designed to amplify 773 bp upstream and 758 bp downstream of the prophage, respectively (**Figure 1b**). These upstream and downstream regions also contain the first 33 and last 95 bp, respectively, of SfPat. Flanking primers EDK81/82 were used for PCR screening of candidate colonies for SfPat deletion. The flanking primers produce a product of 1697 bp in the event of a successful deletion but otherwise yield a product over 10 kb between the flanking regions, which is a negative reaction under our PCR conditions. The full genomes of all strains were re-sequenced by Illumina sequencing (MiGS, University of Pittsburgh) to confirm the absence of additional genetic changes or mutations in either the upstream or downstream flanking regions of the deletion mutants **(Figures 1a and b).**

Fluorescent strains

Plasmids encoding fluorescent proteins were constructed using *E2 Crimson* (red fluorescence) and *egfp* (green fluorescence) genes, via restriction digestion and ligation, to pBBR1-MCS [56, 57]. The electroporation protocol was adapted from Corts *et al* [58]. Competent cells were made using 3 ml log-phase cultures of *S. fidelis* JG4066 and JG4063. The resulting cultures were pelleted by centrifugation and washed three times with 1M sorbitol and resuspended in 150 µL of 1M sorbitol. Plasmids (100 ng) were added to 50 µL of competent cells, and electroporation was carried out at 1.4 kV for 4 msec with 10 µΩ resistance. The transformants were maintained on LB/MB with 17 µg/ml chloramphenicol.

S. fidelis crystal violet biofilm assay

WT and prophage KO strains were cultured in MB overnight at RT, and then diluted to 10^7 cfu/ml in MB. The cultures were brought to 2 ml final volume of MB in 12-well dishes and incubated at RT for 24 hrs to examine biofilm development. Each variable was tested in technical duplicate. Biofilms were quantified by crystal violet staining as previously described [59]. Briefly, supernatants were aspirated after 24-hour incubation and the biofilms were dried and stained with 0.1% crystal violet for 10 mins. The stained biofilms were then gently washed with deionized water, and the amount of biofilm produced was quantified as the intensity of the stain (OD_{570}) after it was extracted from the biofilm with 30% acetic acid. All biofilm assays were performed at least in triplicates.

Motility assay

Soft-agar overlay motility assays were carried out in 12-well dishes to compare swimming behaviors [60, 61]. Briefly, a bacterial colony was cultured overnight at RT and then inoculated onto the center of soft agar (containing LB/MB and 0.5% low-melt agarose) and incubated at RT overnight. The results were recorded as the distance traveled (in millimeters) from the inoculation zone. Each variable was tested in duplicate. Two perpendicular distances (from the inoculation zone) were recorded and averaged for each well.

Congo red assay

A modified Congo red assay was adapted and implemented to infer internal cyclic-di-GMP levels [62]. Briefly, bacteria that were cultured overnight were adjusted to 0.05 OD_{600} in LB/MB with 0.04% Congo red in six-well dishes. After 24 hours, the supernatant was spun down at 8000 g for 1 min. OD_{490} and OD_{750} values were determined. $OD_{750,}$ an infra-red wavelength, was used for subtracting turbidity. LB/MB was used as blank while sterile LB/MB +0.04% Congo red was used as positive control. The value of OD_{490} -OD_{750} of the samples were subtracted from that of the positive control. This value represents the Congo red signal in the supernatant. Experiments were conducted in triplicates, and significance was calculated using an unpaired t-test.

Ciona mariculture

The *in vivo* colonization experiments were performed on animals reared under conditions termed “semi-germ-free” (SGF), which include minimal exposure to marine

microbes. SGF conditions include animals harvested under conventional approaches [63] but permanently maintained in 0.22 µm-filtered, conditioned artificial seawater (cASW), handled with gloves, and lids only carefully removed for water/media changes. cASW is prepared by conditioning ASW made with Instant Ocean™ in an in-house sump-aquarium system containing live rock and growth lights, along with sediment from San Diego, California; salinity is maintained at 32-34 parts per thousand (or grams per liter). Compared to germ-free [64] or SGF approaches, conventionally-reared (CR) includes a step-up exposure to 0.7 µm-filtered cASW that introduces marine bacteria more naturally. The SGF approach is considered an intermediate method of rearing that includes minimal microbial exposures while increasing developmental maturity (unpublished observations). The animals were reared at 20 ^{o}C from larval to juvenile stages. Since *Ciona* adults are acquired from Mission Bay, California to generate juveniles for each of the biological replicates, the wild-harvested animals offer wider genetic diversity than conventional model systems that have had their genetic diversity reduced or eliminated by controlled breeding practices.

Gut colonization assays

All bacterial strains were grown overnight at RT in MB and diluted to 10^7 cfu/ml in cASW after repeated washes. Metamorphic stage 4 (MS4) animals reared in six-well dishes in cASW were exposed to 5 ml of 10^7 cfu/ml bacteria in each well for one hour. MS4 animals are considered part of the 1st ascidian stages (post-settlement stages 1-6, whereas stage 7-8 and onwards are 2nd ascidian stages, and reflect young adult animals). MS4 juveniles can be identified as having a pair of protostigmata, or gill slits,

on each side of the animal [37]. These juveniles first initiate feeding via newly developed and opened siphons; before this, the gut remains closed, and the inside lumen is unexposed to the outside world. Following this initial exposure, or colonization for various time intervals, the plates were rinsed multiple times with cASW and replaced with fresh cASW. Five juveniles were chosen randomly for each treatment, pooled, and homogenized with a plastic pestle; live bacteria were counted by performing serial dilutions and enumerating colony-forming units (cfu) via spot-plating assays [65, 66]. Each of the graphed data represents a biological replicate dataset from genetically distinct/ diverse backgrounds of *Ciona* (represented by separate live animal collection and spawning events). Statistical significance was calculated using Wilcoxon t-test by pooling data across three to six genetically diverse biological replicates.

Live bacteria in the gut were visualized using *Bac*Light stains and previously described fluorescently labeled bacteria [67]. For *Bac*Light staining, 1 ml of bacterial cultures were grown overnight at RT, pelleted, washed twice with cASW, and stained with 4 µl of *Bac*Light Red or *Bac*Light Green for 15 mins in the dark. The stained cultures were washed twice with cASW, and then diluted to 10^7 cfu/ml with cASW. MS4 animals in 6-well dishes were then exposed to 5 ml of this culture. Bacteria in the gut of animals were visualized after one hour on a Leica DMI 6000B stereoscope with a CY5 fluorescent filter for *Bac*Light Red and GFP filter for *Bac*Light Green; and imaged-captured with a Hamamatsu ORCAII camera (model C10600-10B-H) and processed with the MetaMorph 7.10.4 imaging suite (Molecular Devices, Downingtown, PA). Visualization was also done with similar treatments and microscope settings using *Shewanella* 4066 – E2 Crimson and 4063-egfp.

RT-qPCR

To determine if the *Ciona* innate immune system can recognize and respond to the unique mutant strains, which differ only in the presence or absence of the prophages, reverse transcription-quantitative PCR (RT-qPCR) was performed. RNA was extracted using the RNA XS kit (Macherey-Nagel, Düren, Germany) from MS4 *Ciona* juveniles that underwent gut colonization. Complementary DNA (cDNA) synthesis was performed with oligo-dT primers and random hexamers using the First Strand cDNA Synthesis Kit (Promega, Madison WI) following the manufacturer's instructions. Amplification was set up with the qPCR kit (Promega, Madison, WI) and carried out on an ABI7500 with an initial melting temperature of 95°C for 2 mins and 40 cycles of 95°C for 15 sec and 60°C for 1 min. Targeted genes, and their primers, are reported in Table 4. Results from four distinct biological replicates are presented. Each replicate includes pooled *Ciona* juveniles from at least two wells of a 6-well dish. *Ciona* actin was referenced as an endogenous control. Data was analyzed using $\Delta\Delta C_T$ method [68] and the ABI7500 software suite.

To identify candidate bacterial genes that are differentially regulated due to the presence of prophages, bacterial gene expression was studied *in vitro*. The bacterial strains and phage KOs were cultivated in six-well dishes using the same methodology described for biofilm assays. After 24 hours, the supernatant was discarded and RNA from the biofilm was extracted using the Zymo Research Direct-zol kit. cDNA synthesis and qPCR were carried out as described above. As bacterial settlement dynamics differed after deletion of prophages, appropriate regulatory genes were tested and are

listed in Table 4. Rho was identified as the most stable reference gene using RefFinder, which utilizes Bestkeeper, GeNorm, Normfinder and comparative ΔC_T methods (**Figure S2** and Supplementary Table 2) [69-72].

Statistical analysis and data visualization

Statistical analysis and data visualization were carried out in R v4.2 [73]. Data were plotted with ggplot 3.3.5 [74]; the Beeswarm plot was constructed using ggbeeswarm 0.6 [75]. Beeswarm plots and statistics for motility assays were calculated using replicate averages [76]. Statistical significance was calculated using ggsignif package 0.6.3 or ggpubr0.4.0 [77, 78]. If the data were found to be normally distributed by Shapiro's test, then significance was calculated using an unpaired t-test. The Wilcoxon signed-rank test was used to calculate the significance of non-parametric data.

Results

S. fidelis 3313 genome assembly

The *S. fidelis* 3313 genome assembly resulted in 34 contigs totaling 4,901,198 bp with a G+C content of 42.95%. These contigs, span~99.84% of the reference genome with only 0.04% possible contamination as evaluated by CheckM [47]. The two largest contigs (4,824,570 bp and 43,647 bp each) are predicted to encode 98.6% of the genome. Based on CompareM analysis, strain 3313 shares ~99% average amino acid identity with the *S. fidelis* ATCC BAA-318 isolate first identified in sediments of the South China Sea and ~93% of the genes are orthologous. Our previous size prediction

of the two prophages, SfMu1 and SfPat (Table 5), included some adjacent bacterial genomic DNA, indicating SfMu1 to be 45,796 bp [36]. Homology of the integrase gene product supports SfMu1 as a Mu-like phage [79]. Likewise, homology of the capsid proteins indicates that SfPat is a PM2-like phage [80]. These prophages are localized to Contig 1 of the current assembly (**Figure 2**).

A third inducible 60,137 bp prophage, encoding 68 open reading frames (ORFs), was also identified in the improved genome assembly. This third prophage is predicted to be most closely related to the MuSo1 phage component of *Shewanella* FJAT-53749 (accession no. WP_220070840.1) based on the similarity of its integrase, capsid, and protease sequences. Additional prophage ORFs encoding proteins matching MuSo1 include structural proteins, terminase small unit (accession no. KOO57259.1), terminase large unit (accession no. WP_168825185.1), and the Mu-like flu mu region (accession no. KJE44690.1) (Supplementary Table 1). Because of its similarity to the Mu family of phage proteins, this prophage is termed SfMu2. Additional sequence contigs that do not assemble to the main *S. fidelis* 3313 genome include at least three small contigs encoding potential phage ORFs.

Sequence verification of prophage deletion mutant strains

Colony PCR and single primer extension sequencing were both used to validate all deletions, using primers EDK81/82 for SfPat and EDK83/84 for SfMu1 (Table 3). All recovered amplicon sizes were consistent with predictions for SfPat and SFMu1 deletions. The SfMu1 deletion strain was subsequently named JG4005 and the SfPat deletion was named JG3862 (Table 1). SfPat was further deleted from JG4005,

establishing a double mutant, JG4063. Genome sequencing of the deletion mutant strains did not reveal the significant introduction of any mutations or DNA modifications (Supplementary Figure S1a and S1b). These mutant strains were then used for *in vitro* and *in vivo* experiments to understand the potential role of prophages in shaping *S. fidelis* 3313 colonization dynamics in the gut of *Ciona.*

Prophage deletion modulates biofilm formation and motility in *S. fidelis* 3313

Deletion of prophage regions from *S. fidelis* 3313 contributed to an overall increase in biofilm formation as quantified by crystal violet staining (**Figure 3a**). Specifically, we observed that the strains possessing a SfPat deletion alone, or with deletion of both prophages, demonstrate approximately 23% increased biofilm compared to wild-type (WT) strains, p-value of 0.026 and 0.028, respectively (**Figure 3a**). To determine if the changes in biofilm formation is also accompanied by differential motility or chemotaxis in *S. fidelis* 3313, we studied bacterial swimming on simple semi-solid media. Bacterial motility was measured by the spread diameter from a primary inoculation point after an overnight incubation (**Figure 3b**). WT strains demonstrated the largest mean diameter of 8.21 mm. The deletion of SfMu1 and SfPat resulted in decreased diameters of 5.79 mm and 4.04 mm, respectively. Deleting both the prophages resulted in the smallest diameter of 3.58 mm.

We then wanted to see what regulatory mechanisms of bacterial physiology were impacted by the prophages. Bacterial biofilm formation is often regulated by secondary signaling molecules like cyclic-di-GMP (c-di-GMP) [81]. Components of extracellular matrix like exopolysaccharides, curli and/or cellulose are involved in biofilm formation

and known to bind to Congo red, a diazo dye [62]. While the presence of these components have not been shown in *Shewanella*, it has been used as an indirect measure of c-di-GMP in other gram-negative bacteria like *Agrobacterium* and *Pseudomonas* [62, 82] Using this principle, we carried out a Congo red assay to compare the uptake of Congo red by biofilms of the WT and phage-deleted mutant strains. When bacteria grow as biofilms in media containing Congo red, the dye is preferentially retained in the biofilm. Hence, less of the dye will be present in the supernatant and quantified by optical density. We found that Congo red was lower in the supernatant of the double KO mutant strain with enhanced biofilm formation, suggesting an increased production of compounds regulated by c-di-GMP (**Figure 3c**). Since swimming and biofilm formation behaviors are also dependent on quorum sensing mechanisms, we measured changes in the expression levels of genes regulating c-di-GMP by qPCR; three genes, pleD, chitinase and pdeB, were targeted.

The bacterial gene, *pdeB*, encodes a phosphodiesterase enzyme that degrades c-di-GMP and can serve as a negative regulator of motility, positive regulator of biofilm formation, and quorum sensing signal [83]. We performed an *in vitro* experiment using qPCR to quantify the expression of *pdeB* by bacteria recovered from either 24-hour biofilms (*in vitro*). Deletion of any prophages reduced the expression of *pdeB*, but only deletion of both prophages resulted in statistically significant reductions of *pdeB* expression (**Figure 3d**). The other genes did not reveal any statistically significant changes (data not included).

The influence of prophages on *Ciona* gut colonization by *S. fidelis* 3313.

Since motility and biofilm formation are essential to shaping the structure of bacterial communities that associate with animals, we investigated whether prophages could impact the ability of *S. fidelis* 3313 to colonize the *Ciona* gut. Colonization assays were performed on MS4 *Ciona* juveniles by exposing animals to individual WT and mutant strains as described above, repeating the experiments three times across juveniles of diverse genetic backgrounds, i.e., using gametes from distinct outbred adults.

MS4 *Ciona* juveniles were exposed for one hour to *Bac*Light Green-stained WT and *Bac*Light Red-stained double KO mutant variants. These experiments revealed differential localization to the stomach epithelium by the double KO strain and the esophagus by the WT variant (**Figure 4a**). Since *Bac*Light is a vital dye that interacts with surface peptidoglycans, the experiment was also repeated with the same strains transformed to carry and express plasmids encoding fluorescent markers; e.g., WT strain carrying a plasmid encoding E2 Crimson and the double KO strain carrying a plasmid encoding EGFP (**Figure 4b**). The results of both experiments were identical.

One hour after exposure to the mutant strains, bacteria were recovered from animals and quantified by counting colony-forming units (cfu). Experiments were repeated on three separate occasions using juveniles from diverse genetic backgrounds (**Figure 4 c-e**). Retention of the double KO strain was consistently lower, 0.44-to-0.724-fold, compared to the WT strain. The SfPat KO revealed a statistically insignificant 1.3-to-1.5-fold increase in retention in all three rounds. The retention of SfMu1 KO was highly variable. Overall, each round gave similar trends **(Figure 4c-e)**, but these

differences were not statistically significant when the data were pooled (Wilcoxon test, **Figure 4f**). Gut colonization dynamics between WT and ΔSfPatΔSfMu1 were also compared for various time points ranging from 1 hour to 24 hours (Supplementary Figure S3). At the 4 hr time point, the WT was significantly more abundant in the gut of MS4 animals, as compared to the double KO strain.

Host immune discrimination of prophage KO mutant strains

To determine if host immunity discriminates among *S. fidelis* 3313 strains differing only in the presence or absence of prophages, we examined the expression patterns of immune-related genes, such as interleukin-17 and IL17 receptor, complement component 3a (C3a) receptor, NFκ–B, tumor necrosis factor alpha (TNFα), and mannose-binding lectin (MBL) [84]. We also tested VCBP-C, a secreted immune effector expressed in the gut epithelium of *Ciona* [85], can bind (and opsonize) bacteria within the gut lumen [42], and influence biofilms *in vitro* [43]. After one hour of exposure to the *S. fidelis* 3313 mutant strains, changes were detected in the expression of VCBP-C. Up-regulation was noted when juveniles were exposed to phage KO mutant strains of *S. fidelis* 3313, compared to the WT strain (**Figure 5a**) by qPCR. For example, a significant three-fold overexpression (p-value 0.042) of VCBP-C was noted in *Ciona* exposed to the double KO compared to those exposed to the WT strain. Statistically significant two-fold increases in VCBP-C expression were also noted in *Ciona* juveniles exposed to the individual phage KOs mutant strains compared to colonization with the WT strain.

Additional innate immune components were also examined during colonization of MS4 juveniles by the same mutant strains (**Figure 5b,** Supplemental Figure S4). In experiments with 24 hr exposures and multiple biological replicates, we found that IL17-1, IL17 receptor and VCBP-C gene expression were upregulated in WT as compared to the double KO across multiple biological replicates; this pattern of VCBP-C expression is distinct from what was noted after 1 hr of exposure (see above; **Figure 5a**).

Discussion

In this study, a nearly completed genome of *S. fidelis* 3313 is provided by combining short- (Illumina sequencing) and long-read assemblies (PacBio sequencing), resulting in improved localization of two known prophages, SfPat and SfMu1. A third prophage, SfMu2, was also identified, and its genomic location was described. Using phage-cured mutants, it was observed that prophages of *S. fidelis* 3313 can result in increased swimming reduced biofilm formation and subsequently reduced c-di-GMP expression. These bacterial phenotypes affect host immune responses and gut colonization dynamics.

Biofilm formation and motility are often regulated by secondary signaling molecules like c-di-GMP [81]. In bacteria, motility and biofilm formation are regulated by the secondary signaling molecule c-di-GMP. Motility is inversely related to c-di-GMP levels while biofilm formation directly correlates with c-di-GMP levels [81]. Congo red binds to components of the biofilm matrix that are regulated by c-di-GMP. The Congo red assay revealed that the double KO mutants likely produce more biofilm components that are known to be regulated by c-di-GMP. This implies that double KO might express

increased amounts of c-di-GMP than WT [62]. We then monitored changes to the levels of an important regulatory enzyme of this dinucleotide. The phosphodiesterase *pdeB* is a known negative regulator of c-di-GMP and its expression has been shown to influence biofilm formation and motility in *S. oneidensis* [83]. We report that the deletion of prophages in *S. fidelis* 3313 results in decreased expression of *pdeB* in KO strains compared to the WT from overnight biofilms. While the same trends of *pdeB* gene expression were observed in bacteria recovered from the guts of MS4 *Ciona*, the combined biological replicates lacked statistical significance. Other factors likely influence bacterial c-di-GMP levels while inhabiting the gut of animals, and these concepts are being explored further.

Our data suggest an increase in the accumulation of c-di-GMP in the double KO mutant strain. Based on these results, we hypothesize that increased c-di-GMP in the prophage KO mutant strains leads to reduced motility and increased biofilm formation. Increased c-di-GMP levels have also been reported to reduce motility and impact biofilm morphology in *Vibrio fischeri* [86]. It has also been reported that the influence of a *Vibrio anguillarum* prophage is repressed by specific quorum sensing mechanisms and that this action increases biofilm formation [87]. Some prophages have also been shown to possess other genes that are responsible for shaping motility of *Pseudomonas aeruginosa* [88].

In this report, we find that prophages of *S. fidelis* 3313 only lead to increased retention in the gut at the 4-hour time point, as compared to the double KO. The influence on bacterial retention in the early hours of colonization could be biologically significant in an animal where water moves across the branchial basket continuously.

Our data also suggest the prophages can influence niche preference in the *Ciona* gut, and that the abundance of lysogens can fluctuate with time (Supplementary Figure S3) . The overall impact of prophages on host colonization may be obscured, in part, by the influence of host genetics as suggested by differential retention rates across *Ciona* from different genetic backgrounds (**Figure 4**). Of note, it was recently reported that the marine lytic phage, HLN01, has no apparent influence on how the bacterial symbiont, *Vibrio fischeri*, colonizes its natural host, the bobtail squid *Euprymna scolopes* [89].

Host immunity also plays an important role in shaping gut homeostasis. Distinct microbes and their antigens and/or metabolites can engage host immune responses [90]. Previously, human secretory immunoglobulin A (SIgA) was found to enhance and favor settlement dynamics of bacteria both *in vitro* and *in vivo* [91-94], raising a basic question as to whether this phenomenon is more widespread among other secretory immune effectors present in mucosal environments of animals [95]. We speculate that while prophages likely impact the behavior of lysogenized bacteria in ways that can influence colonization dynamics, interaction with VCBP-C on the mucosal surface of the *Ciona* gut may further influence settlement behaviors [43, 95]. Importantly, we show here that the presence of prophages leads to a reduced expression of *Ciona* VCBP-C in the first hours of colonization (a biologically relevant time), subsequently increasing with prolonged exposures.

We also observe that prophages stimulate IL17-based innate immune responses in *Ciona*. IL17 is a conserved cytokine [96], and its influence is crucial for mucosal immunity and enhancing barrier defenses and integrity [97]. The pathway is also known to stimulate the production of antimicrobial factors and the recruitment of immunocytes

[97]. In mice, it has been established that cells producing IL17 are important in regulating commensals [98]. We have shown here that WT (prophage-containing) *S. fidelis* 3313 evokes distinct IL17 responses compared to the prophage KO mutant strains (**Figure 5a** and **b**). While IL17 can act upstream of NFκ-B, the data here reveal both genes have opposing regulatory patterns. These results imply that prophage-mediated bacterial stimulation of IL17 acts independently of NFκ-B.

Our findings further support the hypothesis that the presence of prophages can alter the outcome of host colonization and immune response. It remains to be shown if prophages stimulate the production of a bacterial metabolite with immunomodulatory properties, or if the host immune system responds to differences in bacterial behaviors or traits that result from an absence of the prophage influence, such as excess biofilm formation.

Metagenomic sequencing of gut microbes from healthy animals has revealed that temperate lifestyles are prevalent among phages from these ecosystems [99-101], an observation also made in the *Ciona* gut [17].The mechanisms by which prophages shape colonization behaviors among gut bacteria remain unclear. While the data reported here are only based on one bacterial strain that colonizes the *Ciona* gut, we find that lysogenized versions of *S. fidelis* colonize the gut with reduced activation of VCBP-C gene expression. These observations may be more widely applicable since lysogens are so abundant in animal microbiomes.

It remains unclear if VCBPs, which possess broad specificities and can bind a range of bacterial hosts, bind lysogenized bacteria with different affinities than their prophage-free counterparts. Since colonization of animal mucosal surfaces is an

ancient process [35], prophages and their integration into bacterial genomes have likely evolved to provide fitness benefits in these often-challenging environments. Determining the role of animal immunity in these exchanges is of broad interest. Because prophages can also be induced to generate lytic particles that lyse bacteria, they can play a valuable role in indirect protection mechanisms for the host [26, 102, 103]. Prophages can also contribute to the transfer of virulence factors [25, 104]; thus, it is possible that a role in shaping colonization dynamics is prioritized if it provides fitness benefits to the lysogenized bacteria. Future studies should clarify the relationship between secreted immune effectors and lysogenized bacteria in processes shaping settlement dynamics, which will provide key insights toward gaining a broader understanding of the microbiome and the multifactorial nature of homeostasis.

Author contributions

O.N. designed, executed, and analyzed experiments and wrote and edited the manuscript, S.L.G., N.P., C.G.F.A., B.A.L., A.L., and E.D.K performed experiments and provided feedback and approved the manuscript, M.N.Y., S.J.L., and B.A.L. performed genome sequence analysis, assembly, and provided feedback and approved the manuscript, M.B. and J.A.G. helped interpret data, provided feedback and approved the manuscript, G.A.L. provided reagents, helped design deletion experiments, helped interpret data, and provided feedback and approved the manuscript, and L.J.D. funded most of the project, helped design experiments, interpret data, and helped write and edit the manuscript.

Funding

This project was supported by NSF IOS-1456301 (L.J.D. and M.B.), NSF MCB-1817308 (L.J.D), NSF IOS-2226050/51 (L.J.D. and J.G.), internal awards from the MCOM Deans Office, and the USF Institute for Microbiomes to L.J.D., an NSF GRFP award to B.A.L., and a New Investigator Award to O.N. by USF.

Acknowledgments

The authors would like to acknowledge the expert technical assistance of Anthony Greco and Amanda Garces for transmission electron microscopy, as well as Gary W.

Litman and John P. Cannon for expert feedback and guidance on earlier efforts of the project.

References

1. Li, H., et al., *The outer mucus layer hosts a distinct intestinal microbial niche.* Nat Commun, 2015. **6**: p. 8292.
2. Johansson, M.E., J.M. Larsson, and G.C. Hansson, *The two mucus layers of colon are organized by the MUC2 mucin, whereas the outer layer is a legislator of host-microbial interactions.* Proc Natl Acad Sci U S A, 2011. **108 Suppl 1**: p. 4659-65.
3. Duncan, K., K. Carey-Ewend, and S. Vaishnava, *Spatial analysis of gut microbiome reveals a distinct ecological niche associated with the mucus layer.* Gut Microbes, 2021. **13**(1): p. 1874815.
4. Harrington, V., et al., *Ecology and Medicine Converge at the Microbiome-Host Interface.* mSystems, 2021: p. e0075621.
5. Hornung, B., et al., *Studying microbial functionality within the gut ecosystem by systems biology.* Genes Nutr, 2018. **13**: p. 5.
6. Moran, N.A., H. Ochman, and T.J. Hammer, *Evolutionary and ecological consequences of gut microbial communities.* Annu Rev Ecol Evol Syst, 2019. **50**(1): p. 451-475.
7. Mirzaei, M.K. and C.F. Maurice, *Ménage à trois in the human gut: interactions between host, bacteria and phages.* Nature Reviews Microbiology, 2017. **15**(7): p. 397-408.
8. Shkoporov, A.N. and C. Hill, *Bacteriophages of the Human Gut: The "Known Unknown" of the Microbiome.* Cell Host & Microbe, 2019. **25**(2): p. 195-209.
9. Howard-Varona, C., et al., *Lysogeny in nature: mechanisms, impact and ecology of temperate phages.* The ISME journal, 2017. **11**(7): p. 1511-1520.
10. Lwoff, A., *Lysogeny.* Bacteriological reviews, 1953. **17**(4): p. 269-337.
11. Boling, L., et al., *Dietary prophage inducers and antimicrobials: toward landscaping the human gut microbiome.* Gut Microbes, 2020. **11**(4): p. 721-734.
12. Mills, S., et al., *Movers and shakers: influence of bacteriophages in shaping the mammalian gut microbiota.* Gut Microbes, 2013. **4**(1): p. 4-16.
13. Bondy-Denomy, J. and A.R. Davidson, *When a virus is not a parasite: the beneficial effects of prophages on bacterial fitness.* Journal of microbiology, 2014. **52**(3): p. 235-242.
14. Aziz, R.K., et al., *Mosaic prophages with horizontally acquired genes account for the emergence and diversification of the globally disseminated M1T1 clone of Streptococcus pyogenes.* Journal of bacteriology, 2005. **187**(10): p. 3311-3318.
15. Jiang, S.C. and J.H. Paul, *Significance of Lysogeny in the Marine Environment: Studies with Isolates and a Model of Lysogenic Phage Production.* Microbial Ecology, 1998. **35**(3): p. 235-243.
16. Silveira, C.B., A. Luque, and F. Rohwer, *The landscape of lysogeny across microbial community density, diversity and energetics.* Environmental Microbiology, 2021. **23**(8): p. 4098-4111.
17. Leigh, B.A., et al., *The gut virome of the protochordate model organism, Ciona intestinalis subtype A.* Virus Research, 2018. **244**: p. 137-146.
18. Kim, M.-S. and J.-W. Bae, *Lysogeny is prevalent and widely distributed in the murine gut microbiota.* The ISME Journal, 2018. **12**(4): p. 1127-1141.
19. Allen, H.K., et al., *Antibiotics in feed induce prophages in swine fecal microbiomes.* MBio, 2011. **2**(6).

20. Banks, D.J., B. Lei, and J.M. Musser, *Prophage induction and expression of prophage-encoded virulence factors in group A Streptococcus serotype M3 strain MGAS315.* Infect Immun, 2003. **71**(12): p. 7079-86.
21. Diard, M., et al., *Inflammation boosts bacteriophage transfer between Salmonella spp.* Science, 2017. **355**(6330): p. 1211-1215.
22. Fang, Y., et al., *Induction of Shiga Toxin-Encoding Prophage by Abiotic Environmental Stress in Food.* Appl Environ Microbiol, 2017. **83**(19).
23. Garcia-Russell, N., B. Elrod, and K. Dominguez, *Stress-induced prophage DNA replication in Salmonella enterica serovar Typhimurium.* Infect Genet Evol, 2009. **9**(5): p. 889-95.
24. Maiques, E., et al., *beta-lactam antibiotics induce the SOS response and horizontal transfer of virulence factors in Staphylococcus aureus.* J Bacteriol, 2006. **188**(7): p. 2726-9.
25. Nanda, A.M., K. Thormann, and J. Frunzke, *Impact of spontaneous prophage induction on the fitness of bacterial populations and host-microbe interactions.* J Bacteriol, 2015. **197**(3): p. 410-9.
26. Wang, X., et al., *Cryptic prophages help bacteria cope with adverse environments.* Nat Commun, 2010. **1**: p. 147.
27. Zhang, X., et al., *Quinolone antibiotics induce Shiga toxin-encoding bacteriophages, toxin production, and death in mice.* J Infect Dis, 2000. **181**(2): p. 664-70.
28. Fortier, L.C. and O. Sekulovic, *Importance of prophages to evolution and virulence of bacterial pathogens.* Virulence, 2013. **4**(5): p. 354-65.
29. Hu, J., et al., *Prophage Activation in the Intestine: Insights Into Functions and Possible Applications.* Front Microbiol, 2021. **12**: p. 785634.
30. Lin, W., et al., *Identification of a Vibrio cholerae RTX toxin gene cluster that is tightly linked to the cholera toxin prophage.* Proceedings of the National Academy of Sciences, 1999. **96**(3): p. 1071-1076.
31. Swidsinski, A., et al., *Comparative study of the intestinal mucus barrier in normal and inflamed colon.* Gut, 2007. **56**(3): p. 343-50.
32. Liu, X., et al., *Physiological Function of Rac Prophage During Biofilm Formation and Regulation of Rac Excision in Escherichia coli K-12.* Scientific Reports, 2015. **5**(1): p. 16074.
33. Rice, S.A., et al., *The biofilm life cycle and virulence of Pseudomonas aeruginosa are dependent on a filamentous prophage.* The ISME Journal, 2009. **3**(3): p. 271-282.
34. Gödeke, J., et al., *Phage-induced lysis enhances biofilm formation in Shewanella oneidensis MR-1.* The ISME Journal, 2011. **5**(4): p. 613-626.
35. Dishaw, L.J., et al., *The gut of geographically disparate Ciona intestinalis harbors a core microbiota.* PLoS One, 2014. **9**(4): p. e93386.
36. Leigh, B., et al., *Isolation and characterization of a Shewanella phage–host system from the gut of the tunicate, Ciona intestinalis.* Viruses, 2017. **9**(3): p. 60.
37. Chiba, S., et al., *Development of Ciona intestinalis juveniles (through 2nd ascidian stage).* Zoolog Sci, 2004. **21**(3): p. 285-98.
38. Davidson, B., *Ciona intestinalis as a model for cardiac development.* Seminars in Cell & Developmental Biology, 2007. **18**(1): p. 16-26.
39. Liu, L.-P., et al., *Ciona intestinalis as an emerging model organism: Its regeneration under controlled conditions and methodology for egg dechorionation.* Journal of Zhejiang University SCIENCE B, 2006. **7**(6): p. 467-474.
40. Liberti, A., et al., *Reflections on the Use of an Invertebrate Chordate Model System for Studies of Gut Microbial Immune Interactions.* Frontiers in Immunology, 2021. **12**.
41. Liberti, A., et al., *A Soluble Immune Effector Binds Both Fungi and Bacteria via Separate Functional Domains.* Front Immunol, 2019. **10**: p. 369.

42. Dishaw, L.J., et al., *A role for variable region-containing chitin-binding proteins (VCBPs) in host gut–bacteria interactions.* Proceedings of the National Academy of Sciences, 2011. **108**(40): p. 16747-16752.
43. Dishaw, L.J., et al., *Gut immunity in a protochordate involves a secreted immunoglobulin-type mediator binding host chitin and bacteria.* Nat Commun, 2016. **7**: p. 10617.
44. Liu, X., et al., *Symbiosis of a P2-family phage and deep-sea Shewanella putrefaciens.* Environmental Microbiology, 2019. **21**(11): p. 4212-4232.
45. Bolger, A.M., M. Lohse, and B. Usadel, *Trimmomatic: a flexible trimmer for Illumina sequence data.* Bioinformatics, 2014. **30**(15): p. 2114-20.
46. Wick, R.R., et al., *Unicycler: resolving bacterial genome assemblies from short and long sequencing reads.* PLoS computational biology, 2017. **13**(6): p. e1005595.
47. Parks, D.H., et al., *CheckM: assessing the quality of microbial genomes recovered from isolates, single cells, and metagenomes.* Genome Res, 2015. **25**(7): p. 1043-55.
48. Parks, D., *CompareM: Comparative Genomic Statistics*. 2020: githuv.
49. Aziz, R.K., et al., *The RAST Server: Rapid Annotations using Subsystems Technology.* BMC Genomics, 2008. **9**(1): p. 75.
50. Kieft, K., Z. Zhou, and K. Anantharaman, *VIBRANT: automated recovery, annotation and curation of microbial viruses, and evaluation of viral community function from genomic sequences.* Microbiome, 2020. **8**(1).
51. Roux, S., et al., *VirSorter: mining viral signal from microbial genomic data.* PeerJ, 2015. **3**: p. e985.
52. Arndt, D., et al., *PHASTER: a better, faster version of the PHAST phage search tool.* Nucleic Acids Research, 2016. **44**(W1): p. W16-W21.
53. Akhter, S., R.K. Aziz, and R.A. Edwards, *PhiSpy: a novel algorithm for finding prophages in bacterial genomes that combines similarity- and composition-based strategies.* Nucleic Acids Research, 2012. **40**(16): p. e126-e126.
54. Saltikov, C.W. and D.K. Newman, *Genetic identification of a respiratory arsenate reductase.* Proceedings of the National Academy of Sciences, 2003. **100**(19): p. 10983-10988.
55. Bryksin, A.V. and I. Matsumura, *Overlap extension PCR cloning: a simple and reliable way to create recombinant plasmids.* BioTechniques, 2010. **48**(6): p. 463-465.
56. Barbier, M. and F.H. Damron, *Rainbow Vectors for Broad-Range Bacterial Fluorescence Labeling.* PLOS ONE, 2016. **11**(3): p. e0146827.
57. Kovach, M.E., et al., *pBBR1MCS: a broad-host-range cloning vector.* Biotechniques, 1994. **16**(5): p. 800-2.
58. Corts, A.D., et al., *A new recombineering system for precise genome-editing in Shewanella oneidensis strain MR-1 using single-stranded oligonucleotides.* Scientific Reports, 2019. **9**(1): p. 39.
59. Liberti, A., et al., *A Role for Secreted Immune Effectors in Microbial Biofilm Formation Revealed by Simple In Vitro Assays*, in *Immune Receptors: Methods and Protocols*, J. Rast and K. Buckley, Editors. 2022, Springer US: New York, NY. p. 127-140.
60. Wolfe, A.J. and H.C. Berg, *Migration of bacteria in semisolid agar.* Proc Natl Acad Sci U S A, 1989. **86**(18): p. 6973-7.
61. Kearns, D.B., *A field guide to bacterial swarming motility.* Nat Rev Microbiol, 2010. **8**(9): p. 634-44.
62. Jones, C.J. and D.J. Wozniak, *Congo Red Stain Identifies Matrix Overproduction and Is an Indirect Measurement for c-di-GMP in Many Species of Bacteria*, in *c-di-GMP Signaling: Methods and Protocols*, K. Sauer, Editor. 2017, Springer New York: New York, NY. p. 147-156.

63. Cirino, P., et al., *Laboratory culture of the ascidian Ciona intestinalis (L.): a model system for molecular developmental biology research*, in *Mar. Mod. Elec. Rec. [serial online]*. 2002.
64. Leigh, B.A., A. Liberti, and L.J. Dishaw, *Generation of Germ-Free Ciona intestinalis for Studies of Gut-Microbe Interactions.* Front Microbiol, 2016. **7**: p. 2092.
65. Gaudy Jr, A., F. Abu-Niaaj, and E. Gaudy, *Statistical study of the spot-plate technique for viable-cell counts.* Applied microbiology, 1963. **11**(4): p. 305-309.
66. Miles, A.A., S. Misra, and J. Irwin, *The estimation of the bactericidal power of the blood.* Epidemiology & Infection, 1938. **38**(6): p. 732-749.
67. Boulos, L., *Pré vost M, Barbeau B, Coallier J, Desjardins R. LIVE/DEAD BacLight: application of a new rapid staining method for direct enumeration of viable and total bacteria in drinking water.* J Microbiol Methods, 1999. **37**: p. 77-86.
68. Pfaffl, M.W., *A new mathematical model for relative quantification in real-time RT-PCR.* Nucleic Acids Res, 2001. **29**(9): p. e45.
69. Xie, F., et al., *miRDeepFinder: a miRNA analysis tool for deep sequencing of plant small RNAs.* Plant Mol Biol, 2012.
70. Pfaffl, M.W., et al., *Determination of stable housekeeping genes, differentially regulated target genes and sample integrity: BestKeeper–Excel-based tool using pair-wise correlations.* Biotechnology letters, 2004. **26**: p. 509-515.
71. Andersen, C.L., J.L. Jensen, and T.F. Ørntoft, *Normalization of real-time quantitative reverse transcription-PCR data: a model-based variance estimation approach to identify genes suited for normalization, applied to bladder and colon cancer data sets.* Cancer research, 2004. **64**(15): p. 5245-5250.
72. Vandesompele, J., et al., *Accurate normalization of real-time quantitative RT-PCR data by geometric averaging of multiple internal control genes.* Genome biology, 2002. **3**(7): p. 1-12.
73. Team, R.C., *R : A language and environment for statistical computing.* 2021.
74. Wickham, H., *ggplot2: Elegant Graphics for Data Analysis*. 2016.
75. Eklund, A.T., James, *The Bee Swarm Plot, an Alternative to Stripchart*. 2021: github.
76. Lord, S.J., et al., *SuperPlots: Communicating reproducibility and variability in cell biology.* Journal of Cell Biology, 2020. **219**(6).
77. Kassambara, A., *ggpubr: 'ggplot2' Based Publication Ready Plots*. 2020: github.
78. Constantin, A.-E.P., Indrajeet, *{ggsignif}: R Package for Displaying Significance Brackets for {'ggplot2'}*. 2021: PsyArxiv.
79. Harshey, R.M., *Phage Mu*. 1988, Springer US. p. 193-234.
80. Männistö, R.H., et al., *The Complete Genome Sequence of PM2, the First Lipid-Containing Bacterial Virus To Be Isolated.* Virology, 1999. **262**(2): p. 355-363.
81. Jenal, U. and J. Malone, *Mechanisms of Cyclic-di-GMP Signaling in Bacteria.* Annual Review of Genetics, 2006. **40**(1): p. 385-407.
82. Heindl, J.E., et al., *Reciprocal control of motility and biofilm formation by the PdhS2 two-component sensor kinase of Agrobacterium tumefaciens.* Microbiology, 2019. **165**(2): p. 146-162.
83. Chao, L., et al., *PdeB, a Cyclic Di-GMP-Specific Phosphodiesterase That Regulates Shewanella oneidensis MR-1 Motility and Biofilm Formation.* Journal of Bacteriology, 2013. **195**(17): p. 3827-3833.
84. Marino, R., et al., *Environmental stress and nanoplastics' effects on Ciona robusta: regulation of immune/stress-related genes and induction of innate memory in pharynx and gut.* Frontiers in Immunology, 2023. **14**: p. 1176982.
85. Liberti, A., et al., *An immune effector system in the protochordate gut sheds light on fundamental aspects of vertebrate immunity.* Pathogen-Host Interactions: Antigenic Variation v. Somatic Adaptations, 2015: p. 159-173.

86. Isenberg, R.Y., et al., *High levels of cyclic diguanylate interfere with beneficial bacterial colonization.* Mbio, 2022. **13**(4): p. e01671-22.
87. Tan, D., et al., *High cell densities favor lysogeny: induction of an H20 prophage is repressed by quorum sensing and enhances biofilm formation in Vibrio anguillarum.* The ISME Journal, 2020. **14**(7): p. 1731-1742.
88. Tsao, Y.-F., et al., *Phage Morons Play an Important Role in Pseudomonas aeruginosa Phenotypes.* Journal of Bacteriology, 2018. **200**(22): p. e00189-18.
89. Lynch, J.B., et al., *Independent host- and bacterium-based determinants protect a model symbiosis from phage predation.* Cell Reports, 2022. **38**(7): p. 110376.
90. Rooks, M.G. and W.S. Garrett, *Gut microbiota, metabolites and host immunity.* Nature Reviews Immunology, 2016. **16**(6): p. 341-352.
91. Bollinger, R.R., et al., *Secretory IgA and mucin-mediated biofilm formation by environmental strains of Escherichia coli: role of type 1 pili.* Mol Immunol, 2006. **43**(4): p. 378-87.
92. Thomas, A.D. and W. Parker, *Cultivation of epithelial-associated microbiota by the immune system.* Future Microbiol, 2010. **5**(10): p. 1483-92.
93. Pratt, L.A. and R. Kolter, *Genetic analysis of Escherichia coli biofilm formation: roles of flagella, motility, chemotaxis and type I pili.* Mol Microbiol, 1998. **30**(2): p. 285-93.
94. Donaldson, G.P., et al., *Gut microbiota utilize immunoglobulin A for mucosal colonization.* Science, 2018.
95. Dishaw, L.J., et al., *Immune-directed support of rich microbial communities in the gut has ancient roots.* Dev Comp Immunol, 2014.
96. Roberts, S., et al., *Rapid accumulation of an interleukin 17 homolog transcript in Crassostrea gigas hemocytes following bacterial exposure.* Developmental & Comparative Immunology, 2008. **32**(9): p. 1099-1104.
97. Abusleme, L. and N. Moutsopoulos, *IL-17: overview and role in oral immunity and microbiome.* Oral Diseases, 2017. **23**(7): p. 854-865.
98. Kumar, P., et al., *Intestinal Interleukin-17 Receptor Signaling Mediates Reciprocal Control of the Gut Microbiota and Autoimmune Inflammation.* Immunity, 2016. **44**(3): p. 659-671.
99. Minot, S., et al., *The human gut virome: inter-individual variation and dynamic response to diet.* Genome Res, 2011. **21**(10): p. 1616-25.
100. Minot, S., et al., *Rapid evolution of the human gut virome.* Proc Natl Acad Sci U S A, 2013. **110**(30): p. 12450-5.
101. Reyes, A., et al., *Viruses in the faecal microbiota of monozygotic twins and their mothers.* Nature, 2010. **466**(7304): p. 334-8.
102. Barr, J.J., et al., *Bacteriophage adhering to mucus provide a non-host-derived immunity.* Proc Natl Acad Sci U S A, 2013. **110**(26): p. 10771-6.
103. Wang, X., et al., *Cryptic prophages help bacteria cope with adverse environments.* Nature Communications, 2010. **1**(1): p. 147.
104. Wagner, P.L. and M.K. Waldor, *Bacteriophage control of bacterial virulence.* Infect Immun, 2002. **70**(8): p. 3985-93.
105. Liberti, A., et al., *Chitin protects the gut epithelial barrier in a protochordate model of DSS-induced colitis.* Biology Open, 2018. **7**(1).
106. Liberti, A., et al., *Transcriptional and proteomic analysis of the innate immune response to microbial stimuli in a model invertebrate chordate.* Front Immunol, 2023. **14**: p. 1217077.

Figure Legends

Figure 1. Schematic illustration of deletion strategy. a) Location of upstream, downstream and flanking primers used in the deletion of SfMu1, b) Location of upstream, downstream and flanking primers used in deletion of SfPat.

Figure 2. Schematic representation of the *S. fidelis* 3313 genomes to illustrate the relative positions of each prophage. The figure represents the largest contig after assembly.

Figure 3. Effects of prophages on biofilm and swimming in *S. fidelis* 3313, a) Effect of prophages on *in vitro* biofilm formation over 24 hours quantified with crystal violet assay (n=3), b) Role of prophages in swimming (or chemotaxis) quantified as diameter of growth on soft agar after 24 hours (n=6), and c) Congo red assay to infer levels of cyclic-di-GMP from bacteria grown as biofilm at 24 hours n=3), d) Fold change of *pdeB* with Rho as internal control from 24-hour biofilm (*in vitro*), n=3, (*= p-value<0.05, **= p-value<0.01).

Figure 4. Prophage influence on bacterial colonization of the gut. a) *Ciona* MS4 reveal differential colonization of WT stained with *Bac*Light Green in the esophagus and double KO stained by *Bac*Light Red lines the stomach, b) *Ciona* MS4 reveals WT with E2 Crimson plasmid found in the esophagus while double KO with egfp plasmid lining the stomach. Both visualizations were observed one-hour post-colonization, c-e) Three biological replicates of bacterial colonization from MS4 juveniles exposed to prophage KO variants for one hour, e) Pooled rounds of three biological replicates where no significance is observed for gut colonization, and f) Fold-change of VCBP-C gene expression, with actin as an internal control, in MS4 juveniles exposed to prophage KO variants for one hour (n=4) (*= p-value<0.05, **= p-value<0.01).

Figure 5. Innate immunity is influenced by prophages. a) VCBP-C gene expression in MS4 juveniles after 1-hour exposure to *Shewanella fidelis* strains with and without phages, n=4, b) Innate immune gene expression in MS4 juveniles after 24-hour exposure to *Shewanella* strains with and without phages, n=3.

Data availability

S. fidelis 3313 strains submitted under the BioProject PRJNA903273 on NCBI, accession number SAMN31793880 ID:31793880

Table 1: *S. fidelis* 3313 strains

Organism	Phenotype	Biosample
JG4066	WT	SAMN317993881
JG4005	ΔSfMu1	SAMN317993882
JG3862	ΔSfPat	SAMN317993883
JG4063	ΔSfMu1ΔSfPat	SAMN317993884

Table 2: Plasmids used in the study.

Strains/ Plasmids	Genotype	Source/ Reference
UQ950	*E. coli* DH5α λ(pir) host for cloning; F^- Δ(*argF-lac*)*169* *φ*80*dlacZ58*(ΔM15) *glnV44*(AS) *rfbD1 gyrA96*(NalR) *recA1 endA1 spoT1 thi-1 hsdR17 deoR λpir* $^+$	[54]
pSMV3-ΔSfPat	pSMV3 with 778 bp upstream and 779 bp downstream of flanking regions of SfPat	This study
pSMV3-ΔSfMu1	pSMV3 with 687 bp upstream and 772 bp downstream of flanking regions of SfPat	This study
pBRR1-E2Crimson	E2.Crimson [56] added to pBRR1.MCS[57]	This study
pBRR1-egfp-ChlR	egfp [56] added to pBRR1.MCS[57]	This study

Table 3: Primer sequences used in the construction of prophage knockouts.

Primer ID	Sequence (5'-3')
EDK 73	AAACGGATCCAAGAGTTACTAGTGGCGTTTG
EDK 74	CAAGCTCAAGCCAGTCAAATCAAAGGTAGGT
EDK 75	ATTTGACTGGCTTGAGCTTGTGAACATCG
EDK 76	ACACGAGCTCAAGTTCTGCCAAGTCGTAGG
EDK 77	AAATGGATCCCGATCAGCCTGCTAGTTTATT
EDK 78	ACGGAATAGGTTGAATGCGACTCAGGC
EDK 79	TCGCATTCAACCTATTCCGTCATGTTTAGCC
EDK 80	ACATGAGCTCGATGCAGATAAAGAGCCGTAAA
EDK 81	GTTTATTTTGTGGCAATCGCA
EDK 82	GGTAGCAGTGCTTAAACGAT
EDK 83	AAAAGTGAAGCAGGTCAAGG
EDK 84	GACAGGGCAACTTCAACAAG

Table 4 : Genes targeted and the reverse transcription- qPCR primers used in this study.

Gene	Function	Genbank accession no.	Primer (5'-3')	Reference
VCBP-C	Secreted immune effector in the gut	HQ324151	f-AGACCAACGCCAACACAGTA	[105]
VCBP-C			r-CCCATACATTGCAGCATTTC	
Actin	Cytoskeletal Actin (Reference)	AJ297725	f-CCCAAATCATGTTCGAAACC	[105]
Actin			r-ACACCATCACCACTGTCGAA	

IL17-1	Interleukin 17	NM_001129875.1	f-AGGTTAAGAATCCCTATGGTGC	[106]
IL17-1			r-CAAAGGCACAGACGCAAAGG	
IL17-1 rcptr	Interleukin 17 Receptor	NM_001245045	f-TGTTGGCATGAGTGTTCGGT	
IL17-1 rcptr			r-AGTTGGTTCTGCCCCAAAGT	
NFκ-B	Nuclear factor kappa beta	NM_001078304	f-TGTCGCTTGTCGTCATGGAA	[106]
NFκ-B			r-AACACCCAAGACCGTCGAAA	
TNFα	Tumor Necrosis Factor	NM_001128107.1	f-TTCAGAAAGATTGGACGACGA	[106]
TNFα			r-TCGTTTAGAAATGCTGCTGTGG	
C3a-rcptr	Complement component 3 receptor	NM_001078552.1	f-TTGTAAGCTGGCACAAGGTGT	This study
C3a-rcptr			r-GACCGTAGTCTGGTAGAGGTC	
MBL	Mannose Binding Lectin	NM_001167707.2	f-TTATTGATGGGAAAGTTTGGT	This study
MBL			r-TAACATCTCTGTTCTTGGGTC	
pdeB	Phophodiesterase	NF012772.3	f-GCATCAGGGCTCTTACCAATAG	This study
pdeB			r-GAGGCGGTGATCCTTACAGATA	
RecA	Recombinase – Bacterial Reference gene		f-CGTAGTGGTGCGGTAGATGT	This study
RecA			r-CGCATTGCTTGGCTCATCAT	

Table 5: Identification of prophages in *S. fidelis* 3313 genome

Phage	Contig	Range Start	Range End	Length (bp)	Proteins (number)	Phage type identity (Region showing identity)
SfMu2	1	1630281	1690417	60137	68	Mu (MuSo1)
SfPat	1	2100478	2116061	15584	34	PM2 or unclassified Corticovirus
SfMu1	1	3996436	4023728	27293	21	Mu

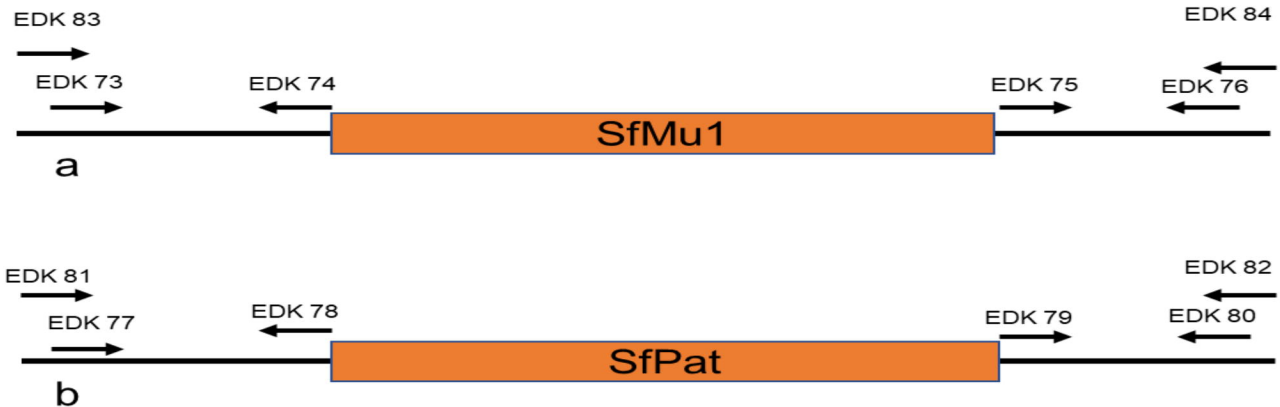
EDK 83
EDK 84
EDK 73
EDK 74
EDK 75
EDK 76
SfMu1
a
EDK 81
EDK 82
EDK 77
EDK 78
EDK 79
EDK 80
SfPat
b

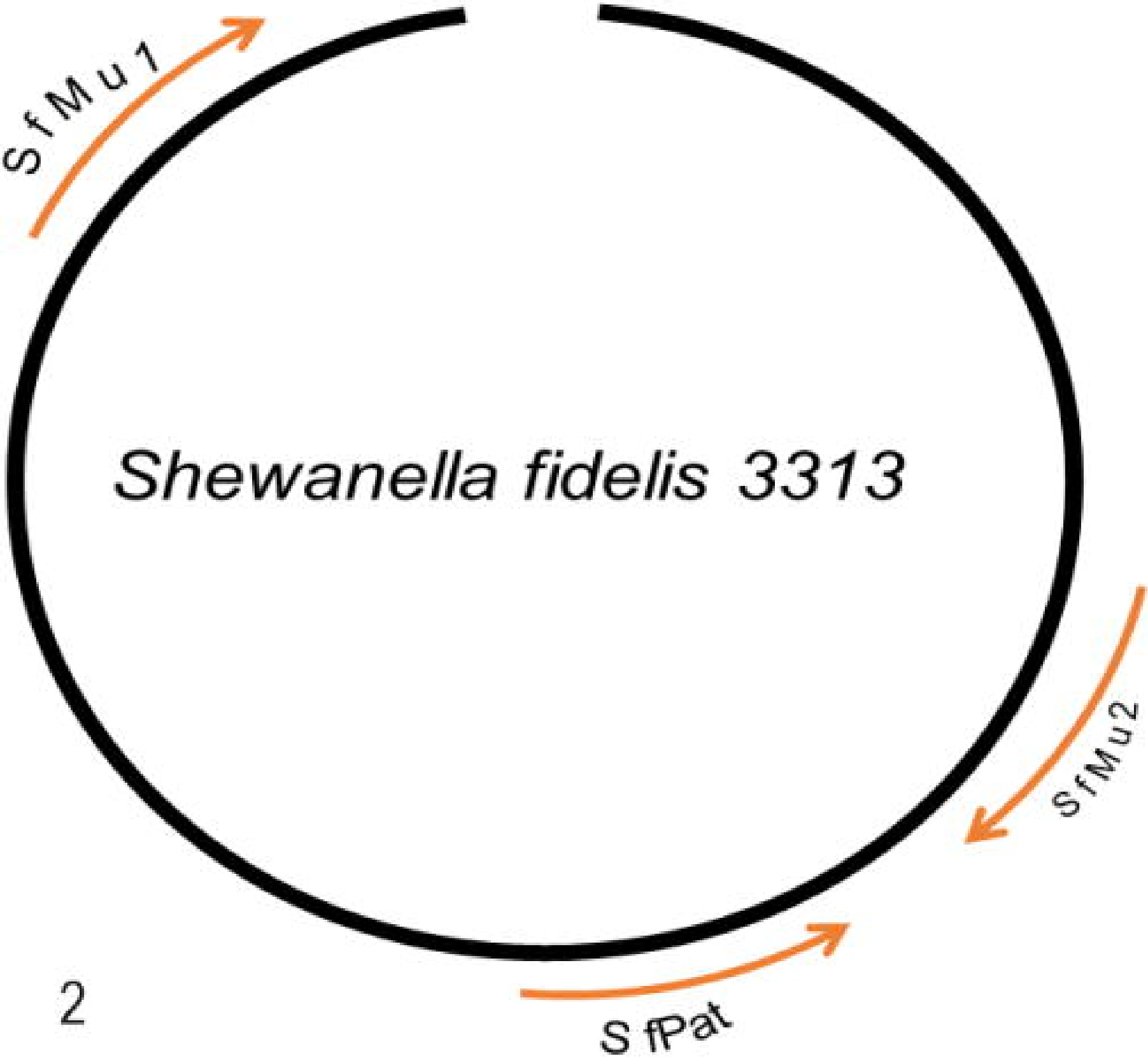
SfMu1
Shewanella fidelis 3313
SfMu2
SfPat

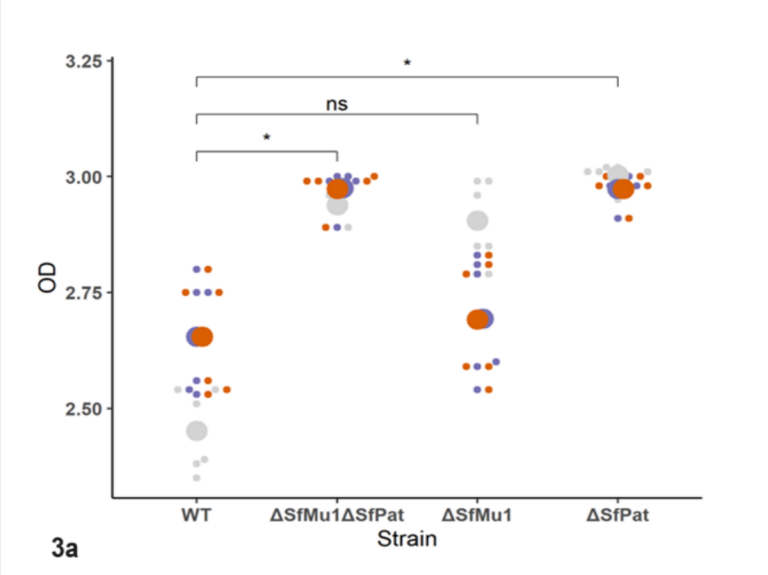
3.25
3.00
2.75
2.50
OD
*
ns
*
WT
ΔSfMu1ΔSfPat
ΔSfMu1
ΔSfPat
Strain
3a

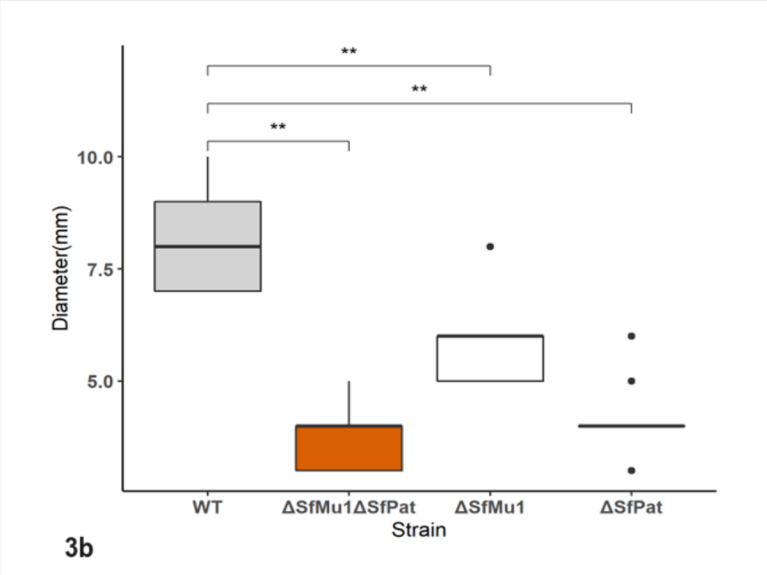
10.0
7.5
5.0
Diameter(mm)
**
**
**
WT
ΔSfMu1ΔSfPat
ΔSfMu1
ΔSfPat
Strain
3b

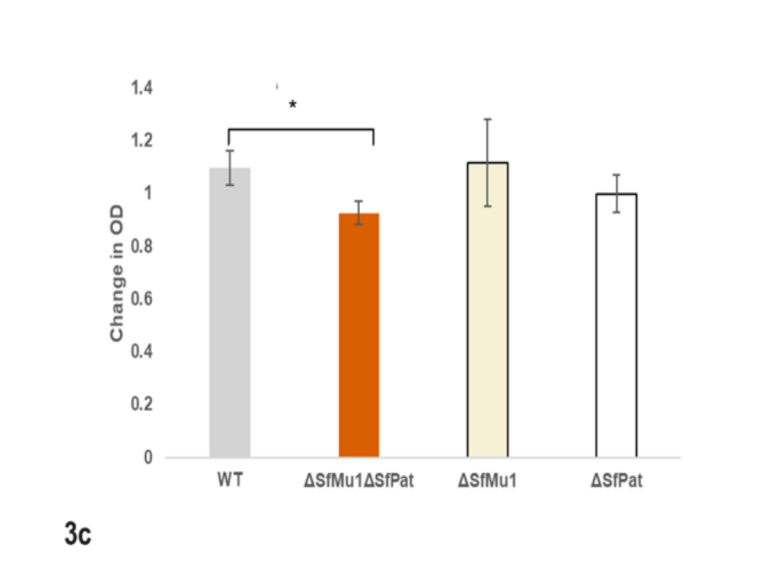
1.4
1.2
1
0.8
0.6
0.4
0.2
0
Change in OD
*
WT
ΔSfMu1ΔSfPat
ΔSfMu1
ΔSfPat
3c

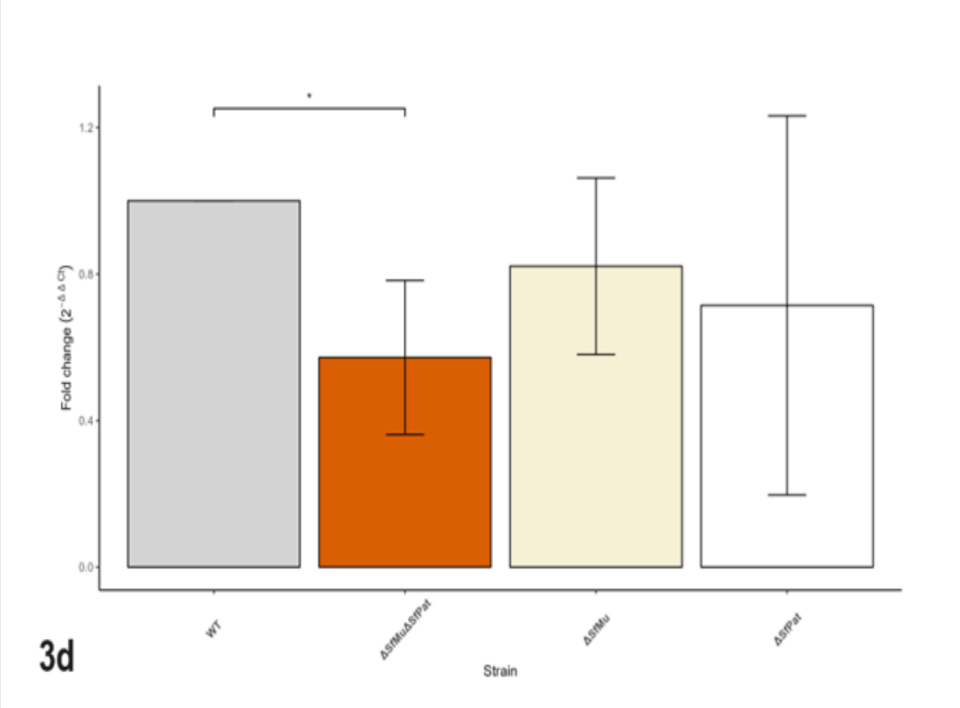
*
1.2
0.8
0.4
0.0
Fold change ($2^{-\Delta\Delta Ct}$)
WT
ΔSfMuΔSfPat
ΔSfMu
ΔSfPat
Strain
3d

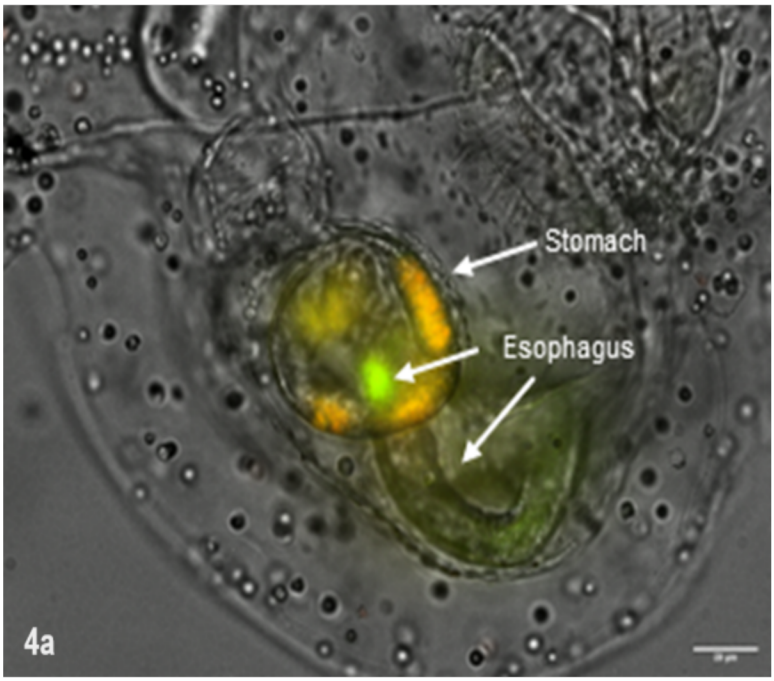
Stomach
Esophagus
4a

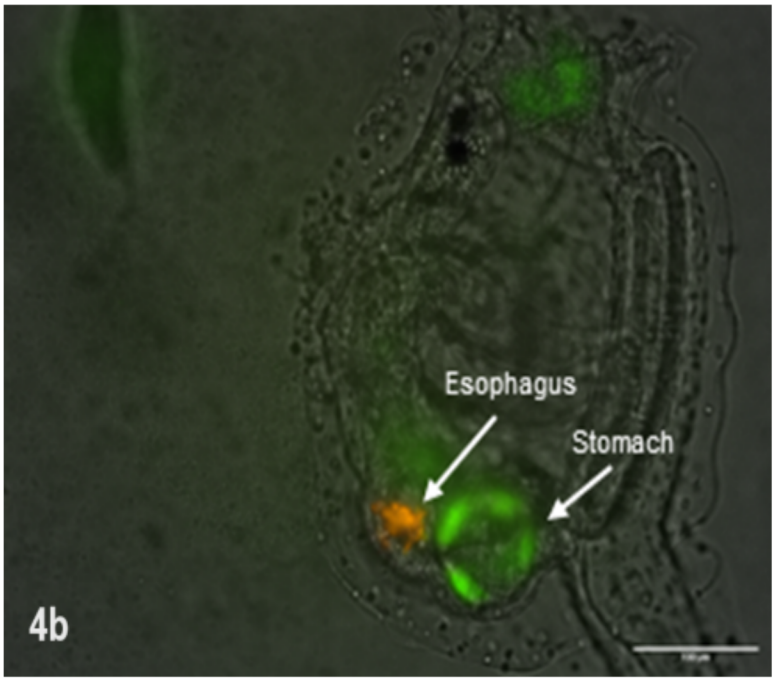
Esophagus
Stomach
4b

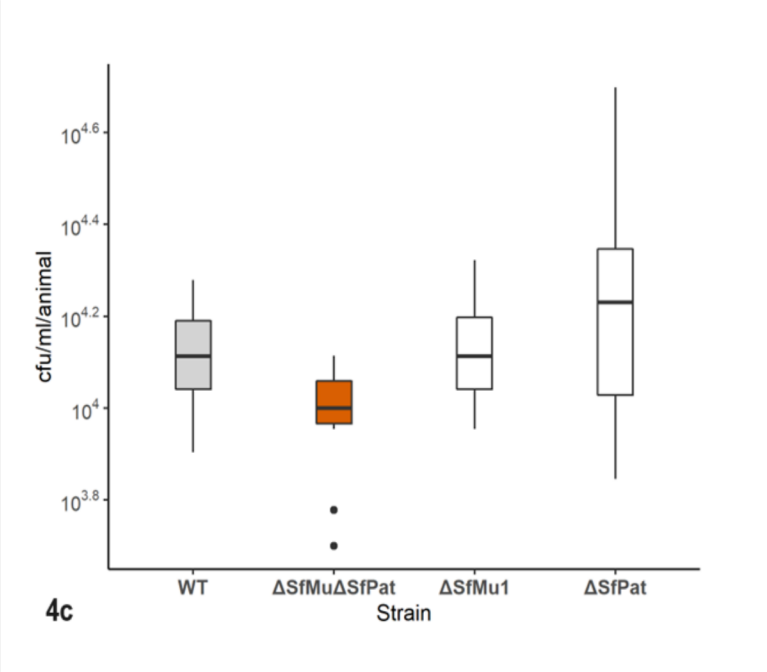
cfu/ml/animal
$10^{4.6}$
$10^{4.4}$
$10^{4.2}$
10^{4}
$10^{3.8}$
WT
ΔSfMuΔSfPat
ΔSfMu1
ΔSfPat
Strain
4c

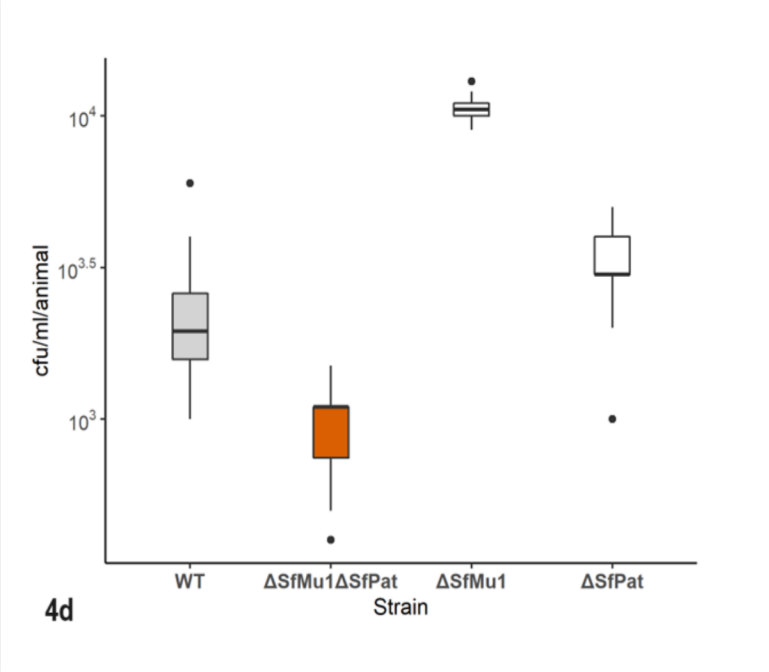
cfu/ml/animal
10^{4}
$10^{3.5}$
10^{3}
WT
ΔSfMu1ΔSfPat
ΔSfMu1
ΔSfPat
Strain
4d

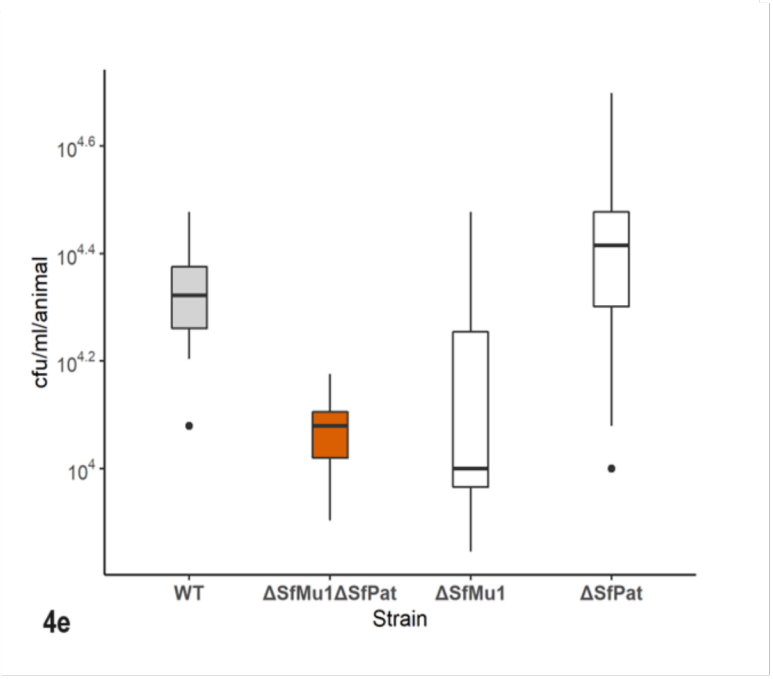
cfu/ml/animal
$10^{4.6}$
$10^{4.4}$
$10^{4.2}$
10^{4}
WT
ΔSfMu1ΔSfPat
ΔSfMu1
ΔSfPat
Strain
4e

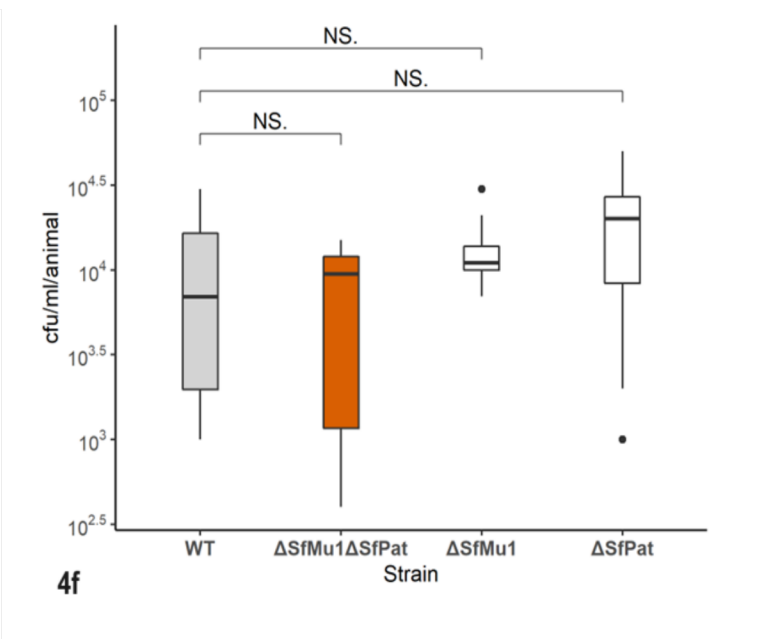
NS.
NS.
NS.
cfu/ml/animal
10^{5}
$10^{4.5}$
10^{4}
$10^{3.5}$
10^{3}
$10^{2.5}$
WT
ΔSfMu1ΔSfPat
ΔSfMu1
ΔSfPat
Strain
4f

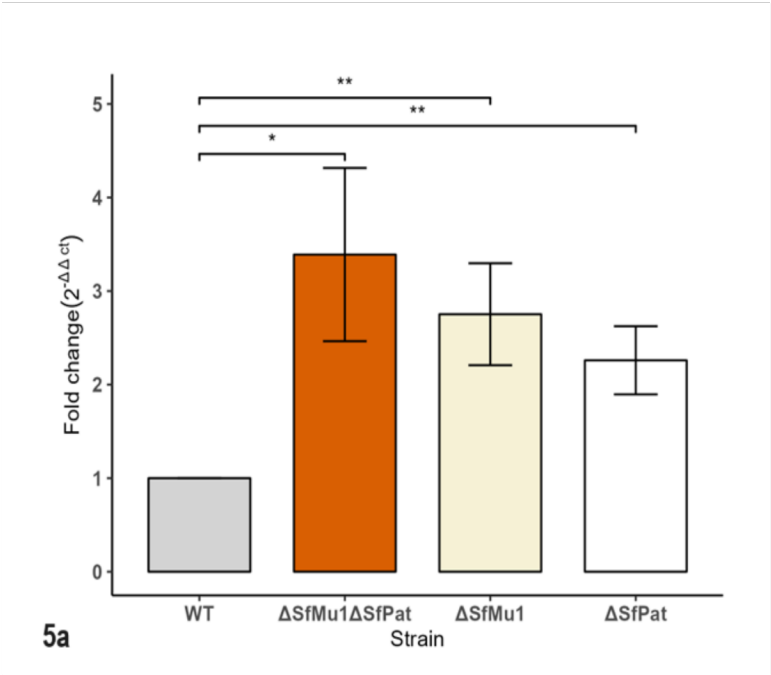
**
**
*
5
4
3
2
1
0
Fold change($2^{-\Delta\Delta ct}$)
WT
ΔSfMu1ΔSfPat
ΔSfMu1
ΔSfPat
Strain

5a

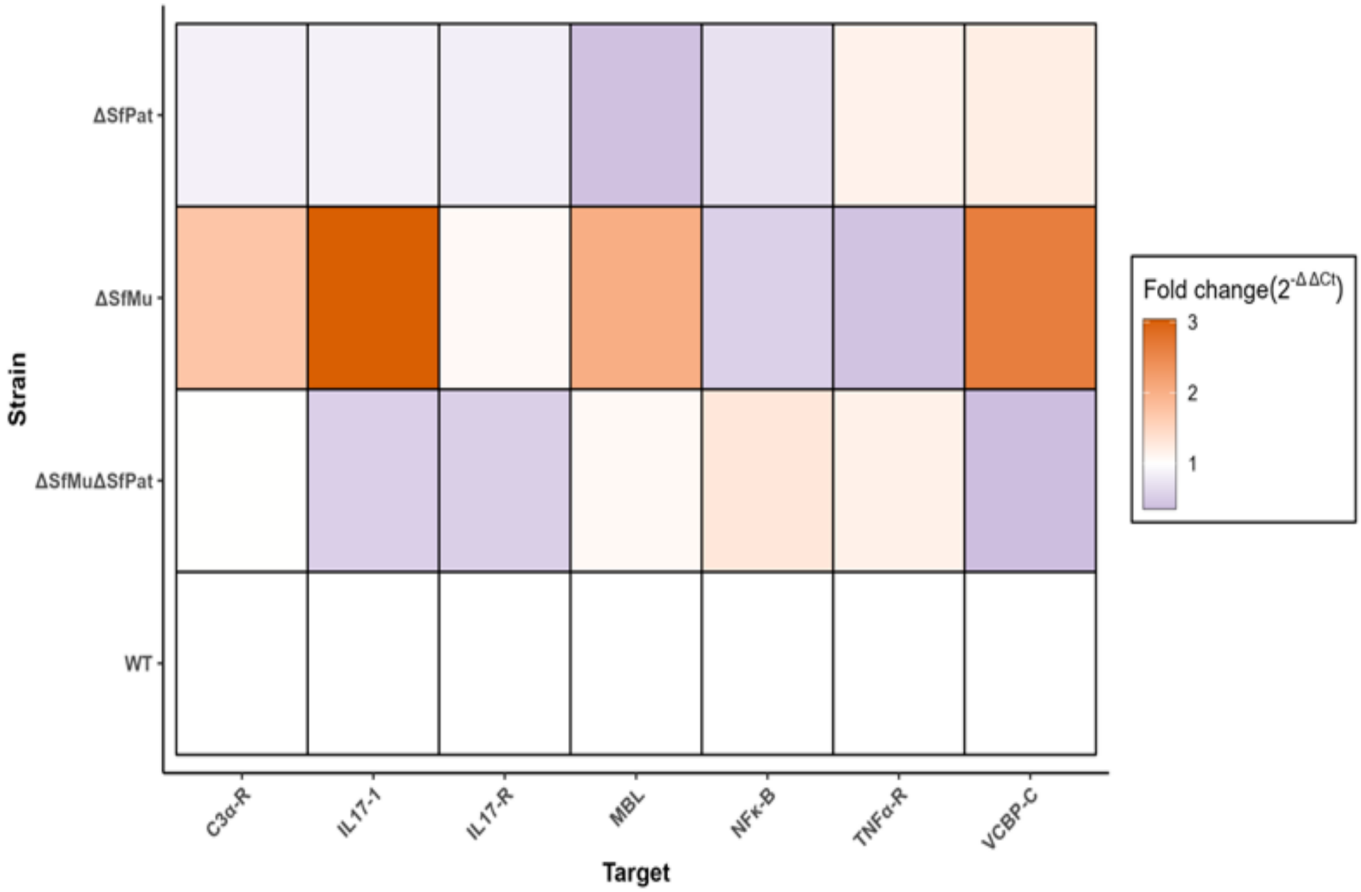
ΔSfPat
ΔSfMu
ΔSfMuΔSfPat
WT
Strain
C3α-R
IL17-1
IL17-R
MBL
NFκ-B
TNFα-R
VCBP-C
Target
Fold change($2^{-\Delta\Delta Ct}$)
3
2
1

5b